Modeling the first stages of Cu precipitation in α-Fe using a hybrid atomistic kinetic Monte Carlo approach

N. Castin,[1,2,a)] M. I. Pascuet,[3,b)] and L. Malerba[1]

[1]*Studiecentrum voor Kernenergie – Centre d'Etudes de l'énergie Nucléaire (SCK CEN), NMS unit, Boeretang 200, B2400 Mol, Belgium*

[2]*Université Libre de Bruxelles (ULB), Physique des Solides Irradiés et des Nanostructures (PSIN), boulevard du Triomphe CP234, 1050 Brussels, Belgium*

[3]*Consejo Nacional de Investigaciones Científicas y Técnicas (CONICET), Av. Rivadavia 1917, C1033AAJ Buenos Aires, Argentina*

We simulate the coherent stage of Cu precipitation in α-Fe with an atomistic kinetic Monte Carlo (AKMC) model. The vacancy migration energy as a function of the local chemical environment is provided on-the-fly by a neural network, trained with high precision on values calculated with the nudged elastic band method, using a suitable interatomic potential. To speed up the simulation, however, we modify the standard AKMC algorithm by treating large Cu clusters as objects, similarly to object kinetic Monte Carlo approaches. Seamless matching between the fully atomistic and the coarse-grained approach is achieved again by using a neural network, that provides all stability and mobility parameters for large Cu clusters, after training on atomistically informed results. The resulting hybrid algorithm allows long thermal annealing experiments to be simulated, within a reasonable CPU time. The results obtained are in very good agreement with several series of experimental data available from the literature, spanning over different conditions of temperature and alloy composition. We deduce from these results and relevant parametric studies that the mobility of Cu clusters containing one vacancy plays a central role in the precipitation mechanism. © *2011 American Institute of Physics*. [doi:10.1063/1.3622045]

I. INTRODUCTION

Copper was inadvertently included as alloying element in nuclear reactor pressure vessel steels of second generation. Later, the formation of Cu-rich precipitates revealed itself as one of the major causes of degradation of mechanical properties in ferritic steels under neutron irradiation[1] (mainly hardening and embrittlement), which is nowadays an important factor limiting the lifetime of nuclear power plants. For this reason, Cu precipitation in α-Fe has been intensively studied during the last decades, both experimentally,[2–7] and using theoretical models[5,8–11] or computer simulations, in particular using atomistic kinetic Monte Carlo (AKMC) techniques.[7,12–15]

The main features of AKMC models and their different applications are reviewed in Refs. 16 and 17. In AKMC simulations of thermal ageing, a single vacancy is introduced in a volume filled with atoms of different chemical species, located on perfect crystal lattice positions. The vacancy acts as vehicle for atomic species redistribution, via thermally activated diffusion jumps, i.e., exchanges of position between the vacancy and an atom nearby. The physics of the model is contained in the activation energies of the diffusion jumps (migration energies of the vacancy), which vary significantly depending on the local chemical, or atomic, environment.

Generally AKMC models are subsumed as rigid lattice models, i.e., crystallographic changes cannot be described. This seems to rule out their use to describe precipitation of face-centered-cubic (fcc) Cu in body-centered-cubic (bcc) α-Fe. However, Cu precipitates in α-Fe are experimentally found to be coherent with the bcc-Fe matrix, up to a diameter between 4 and 5 nm.[18,19] Growing further, they first take intermediate crystallographic structures (first 9R, then 3R) and finally become fcc when they reach diameters above 12 nm.[18,19] This finding was also confirmed using molecular dynamics simulations, which moreover suggested that the stability of Cu precipitates is enhanced by the presence of vacancies inside.[20] Thus, it makes sense to simulate by AKMC the coherent stage of Cu precipitation in Fe, as long as Cu precipitates remain smaller than ∼5 nm.

AKMC models differ from each other essentially by the methodology employed to calculate the migration energies. In most models, they are calculated without allowing for atomic relaxation, using an interatomic potential or fitted pair interaction energies, for example, in a broken-bonds formalism, within a range of interaction of first or second nearest neighbor distance. In some cases, the pair interaction energies are fitted to data calculated with first principles methods. For a critical review of most existing approaches that have been applied for the study of Cu precipitation in Fe, the interested reader is referred to Vincent *et al.*[7] The conclusion by Vincent *et al.* is, however, that none of the models reviewed can consistently predict Cu precipitation in Fe: depending on the parameterization, either the average precipitate radius, or the

---

a)Author to whom correspondence should be addressed. Electronic mail: ncastin@sckcen.be.

b)Electronic mail: pascuet@cnea.gov.ar.

precipitate density is correctly predicted, but hardly ever both. In particular, most models tend to overestimate the density.

Soisson and Fu[15] achieved a more satisfactory and consistent prediction. In their AKMC model, the vacancy migration energy was calculated using a broken-bonds formalism, fitted to energy data calculated by density functional theory. With this model they were able to predict accurately the first stages of Cu precipitation, in terms of both mean precipitate radius and precipitate density. The main reason for their success is probably that their model incorporated a very strong interaction between vacancies and Cu clusters, with the consequence that Cu clusters of all sizes were mobile, via complex series of vacancy hops at or near their surface. They also observed direct coalescence of clusters, as the result of migration. Their results, therefore, suggest that the mobility of Cu clusters, as a consequence of strong interaction with vacancies, can play a non-negligible role in the kinetics of Cu precipitation in Fe. Mobility of Cu clusters was also observed in previous AKMC simulations, though limited to the smallest ones.[12,14] The diffusion of Cu clusters, on the other hand, had never been considered as mechanism in classical diffusion theory models for Cu precipitation.[5,9–11]

The main limitation of Soisson and Fu's model was a "collateral effect" of the strong binding between Cu clusters and vacancy: the latter remained trapped in the bulk of these clusters for a very large fraction of the simulation time, thereby increasing enormously the CPU cost and, therefore, limiting drastically the reach of the simulation, which had to be stopped at a very early stage of the coherent precipitation. Thus, in their work they could not fully assess the consequences of Cu clusters mobility on the kinetics of the precipitation process.

In this work, we simulate Cu precipitation in α-Fe with an AKMC computer simulation approach that allows us to prove clearly that indeed the mobility of Cu clusters is the key to explain the experimentally observed kinetics of precipitation. Classical coarsening mechanisms, such as the progressive growth of large precipitates at the expenses of the dissolution of small ones, by emission of single Cu atoms, would result in a significantly slower precipitation kinetics in terms of size, with density overestimation.

Our AKMC approach is described in ample detail elsewhere.[21] To summarize briefly, we calculate the vacancy migration energies with the nudged elastic band (NEB) method,[22,23] using an interatomic potential, thereby fully allowing for effects of long-range chemical interaction and static relaxation. However, to allow fast estimation of the migration energies during the simulation, the NEB values are in fact provided by a properly trained artificial neural network (ANN).[24] Key for the physical reliability of the model is the quality of the interatomic potential. The Fe-Cu potential we use here was developed in Ref. 25, specifically to fulfill two major objectives: (1) be consistent with thermodynamics, by providing a correct prediction of the experimental Fe-Cu phase diagram and (2) provide an accurate description of the interaction between point defects in α-Fe and Cu atoms. The potential has been proven to be able to predict the correct final equilibrium for a thermal annealing experiment.[25,26] Its ability to fully predict also the kinetic path

from a random solid solution is demonstrated in the present work.

In this work we added a new feature to our model, namely, we combined the full AKMC approach with a coarse-grained approach, of object kinetic Monte Carlo (OKMC) type.[27] Clusters of Cu atoms *above a certain size* are considered as objects, for which migration and dissociation events are defined, based on specific, size-dependent, and thermally activated frequencies. Seamless matching between the fully atomistic model used to describe small Cu clusters and the coarser-grain model used to describe larger Cu clusters is guaranteed by calculating the diffusion coefficients and emission probabilities for the object-like clusters based on specific, full AKMC simulations, on which another ANN has been trained. This "hybrid" AKMC approach proves both computationally efficient and physically very accurate, thanks also to the high quality of the interatomic potential, which is here exploited in the most complete way possible. This enabled us to push our simulations well into the coarsening stage, allowing full comparison with available experimental data. Our model bears some resemblance to the 2D model proposed in Ref. 28.

The paper is organized as follows. In Sec. II, we summarize the fundamentals of our ANN-based AKMC algorithm, reporting in detail on the modifications introduced to "hybridize" it with an OKMC approach. In Sec. III, the hybrid AKMC is used to simulate several thermal annealing experiments in Fe-Cu, for different Cu contents and at different temperatures. Finally, in Sec. IV, we analyze the mechanism of Cu precipitation that stems from our simulations, emphasizing in particular the key role of the diffusion of Cu clusters and precipitates.

II. HYBRID ATOMISTIC KINETIC MONTE CARLO APPROACH

As anticipated in the introduction, in AKMC models atoms are located on the positions corresponding to the crystallographic structure of interest, generally on a rigid lattice. The evolution of the system is driven by the diffusion jumps of vacancies. The jump to occur is selected stochastically each time, according to the jump frequencies,

$$\Gamma = \Gamma_0 \exp\left(\frac{-E_m}{k_B T}\right). \qquad (1)$$

Here, Γ_0 is the attempt frequency, E_m is the migration energy calculated at zero temperature, k_B is Boltzmann's constant, and T is the absolute temperature. The Monte Carlo time increment is then obtained using the standard residence time algorithm.[29–31]

The simulation volume is a cubic and periodic bcc monocrystal, with Fe as matrix. A number of Cu atoms are introduced, according to the alloy composition, as well as one vacant site. An ANN was trained to predict the vacancy migration energy, as calculated with NEB using the potential from,[25] given as input a description of the vacancy local chemical environment (i.e., how Cu atoms are distributed around it). The methodology we followed to train the ANN is fully described in Ref. 21. Figure 1 shows that the predictions are very accurate; therefore, the ANN can be considered
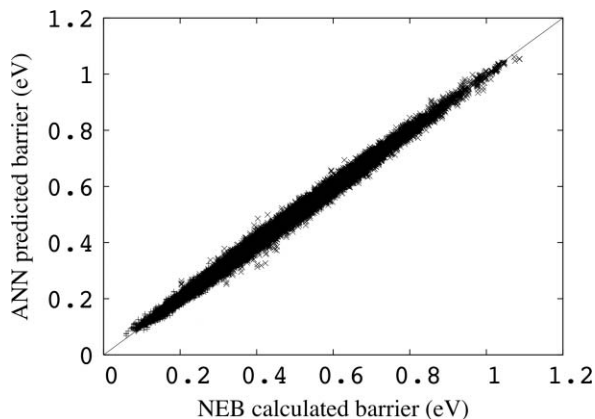
FIG. 1. Quality of the ANN predictions of the vacancy migration energies obtained with the NEB method in Fe-Cu alloys. The input variables are a description of the vacancy local atomic environment up to the 11th nearest neighbors. The average error of predictions is 2.0%, and Pearson's product-moment correlation coefficient R^2 is 0.998.

FIG. 2. Schematic representation of the absorption of a vacancy in a Cu_N cluster in the hybrid AKMC algorithm. Dashed lines represent the radius of the cluster and the absorption radius. On the left side, the vacancy is approaching the cluster and is considered absorbed when a migration event is chosen involving one atom of the cluster. After absorption of the vacancy, Cu atoms situated within the absorption range are immediately absorbed in the cluster, and the new radii are increased accordingly, as shown on the right side.

as an adequate substitute of the computation on-the-fly of energy barriers with NEB. The attempt frequency in Eq. (1) is considered constant and taken to be of the order of Debye's frequency: $\Gamma_0 = 6 \times 10^{12}$ s^{-1}.

Due to the negligible solubility of Fe in Cu, the clusters formed during the simulation are from the beginning completely pure and compact, similar to the findings by other authors in previous AKMC simulations[7,14,15] (clusters are defined by groups of solute atoms that are linked by 1nn or 2nn bonds). Also consistently with previous work, in a full AKMC simulation with this method, the vacancy is strongly attracted by Cu clusters, and remains trapped inside them for a very large fraction of the AKMC events. The simulation is, therefore, significantly slowed down.[7,15] To speed up the calculation, clusters of Cu atoms (henceforth denoted as Cu_N, N being the number of atoms in the cluster) above a certain size ($N \geq N_{min}$) are defined as *objects*, using the approximations described in what follows.

When the vacancy approaches a Cu_N object, as depicted in Fig. 2, the full AKMC algorithm is still applied: possible events are only the migration of the vacancy to a first nearest neighbor position, and the corresponding migration energies are calculated using the ANN shown in Fig. 1. We, therefore, do not introduce any coarse-grain approximation for the migration path followed by the vacancy in the vicinity of a Cu_N cluster, and – most importantly – for the mechanisms of dragging individual Cu atoms, or small Cu clusters, in the direction of the large cluster.

When the vacancy enters in contact with a cluster, many events that would take place in a full AKMC simulation are ignored and replaced by coarse-grain approximations, as shown in Fig. 2. In particular, the most probable outcome of the capture of a vacancy by the cluster is the subsequent inclusion in the cluster of all Cu atoms that are in solution in the matrix, but sufficiently close to the interface with the precipitate to be dragged inside by the vacancy hopping at this interface. To allow for this atomic-level process, we define a spherical absorption radius (radius of the cluster augmented by the 2nn distance) and make the assumption that all
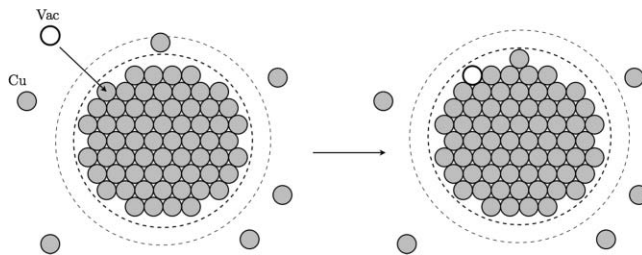
Cu atoms within this radius are immediately absorbed by the cluster.

After the vacancy (v) has been absorbed by a Cu_N cluster object, the latter becomes a vCu_N object, and new events are defined in replacement of the vacancy migration in the regular AKMC algorithm:

- Dissociation of the cluster, with a frequency denoted as $\Gamma_N^{(diss)}$, as depicted in Fig. 3. Two dissociation mechanisms are possible: (i) emission of the vacancy from the cluster or (ii) emission of a vCu_1 pair, as in OKMC simulations.[27] A single frequency for the dissociation is assigned, and the emission of a vCu_1 pair occurs with a probability p_N.
- Migration of the cluster, with a frequency denoted as $\Gamma_N^{(mig)}$. For convenience, we only consider jumps of the central atom of the cluster (dragging the whole cluster) to any of the eight possible 1nn lattice sites (in bcc). After the migration is completed, Cu atoms within the absorption range are added to the cluster.
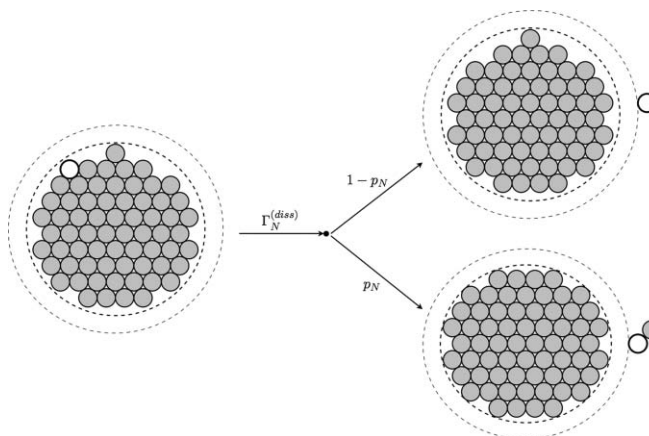- Coalescence of clusters when, after a migration event is chosen, the absorption range of the vCu_N cluster

FIG. 3. Schematic representation of the dissociation event for a vCu_N cluster in the hybrid AKMC algorithm. The frequency of occurrence is denoted $\Gamma_N^{(diss)}$. When applied, the vacancy alone is emitted outside the absorption range (delimited by the dashed lines on the figure). A Cu atom is also emitted occasionally, with a probability denoted as p_N.

overlaps with the absorption range of another Cu_N cluster.

To summarize, the hybrid AKMC algorithm is a compromise between AKMC and OKMC: the description at the atomic level of the system is retained as long as the vacancy is not trapped in Cu_N clusters. In the latter case, vCu_N clusters are defined as objects, and treated in a similar way as in OKMC methods. Clearly, the application of this algorithm requires the pre-definition of values for $\Gamma_N^{(diss)}$, $\Gamma_N^{(mig)}$, and p_N as functions of the size, N, and temperature, T. These values must guarantee seamless matching with the atomistic description. The procedure to obtain this parameterization is described in Sec. II A.

A. Parameterization

First of all, an appropriate threshold value, N_{min}, above which clusters are considered as objects must be chosen. A sensible choice is, e.g., $N_{min} = 15$, because it corresponds, in bcc, to a central atom surrounded by other atoms filling completely its first and second shells of close neighbors (so it is very stable), and it is larger than the critical size for nucleation of Cu clusters in our AKMC. It is also useful to define the maximum allowed size for Cu_N clusters, N_{max}, to remain in a framework of coherent precipitation: $R = 2.5$ nm (Refs. 18 and 19) corresponds to $N_{max} \approx 6000$.

Migration and dissociation of Cu clusters are complex processes that are not easily described with simple formalisms, because they are the consequence of a succession of many vacancy jumps at their surface. We, therefore, use again a numerical approach: cluster migration and dissociation frequencies are estimated with series of independent full AKMC simulations, using the ANN of Fig. 1. The vCu_N cluster is introduced alone in an otherwise pure Fe matrix. The full AKMC algorithm is applied until the vacancy, or a vCu_1 pair, is emitted from the cluster (time to dissociation, or lifetime). Repeating this simulation a large number of times, enough statistics can be collected to calculate the cluster diffusion coefficient D_N, and the average lifetime τ_N, following the procedure described in Ref. 32. The dissociation frequency is the inverse of the lifetime:

$$\Gamma_N^{(diss)} = \frac{1}{\tau_N}. \tag{2}$$

Neglecting correlations, the migration frequency can be derived from the diffusion coefficient using the relationship

$$\Gamma_N^{(mig)} = \frac{6 D_N}{\Delta^2} \cdot \frac{1}{8}, \tag{3}$$

where Δ^2 is the square of the jump distance, i.e., of the 1nn distance, equal to $(3/4)a_0^2$ (a_0 is the lattice parameter, 2.86 Å for dilute Fe-based alloys). The factor 1/8 is introduced to account for the eight possible destinations of migration.

D_N and τ_N are calculated at several very high temperatures (up to 4000 K) and linearly extrapolated down to the temperatures of interest via Arrhenius plots: $\ln(D_N)$ or $\ln(\tau_N)$ versus the reciprocal temperature $1/k_B T$. As a matter of fact, high temperatures make the lifetime, and therefore the simulation time, shorter, thereby enabling the collection of statis-
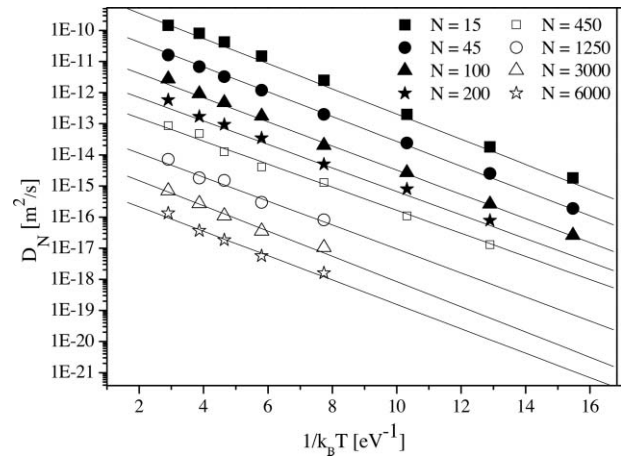

FIG. 4. Diffusion coefficients D_N of different vCu_N clusters versus reciprocal temperature ($1/k_B T$), measured with AKMC simulations. Plain lines show interpolation and extrapolation on the reciprocal temperature using f_1 defined in Eq. (4).

tically relevant quantities of data points, also for very large cluster sizes. A few sets of data points are represented as Arrhenius plots in Figs. 4 and 5. Figure 6 shows an example of diffusion coefficient D_N for $T = 773$ K versus size. We see that for $N > 1000$, the value is not monotonously decreasing with N: these oscillations are entirely attributed to extrapolation errors from high temperature, as indicated by the error bars. In order to fit a function providing diffusion coefficients and lifetime of clusters as functions of both cluster size and temperature, we sought for smooth mathematical expressions to these relationships:

$$\ln(D_N(T)) = f_1(N, 1/k_B T), \tag{4}$$

$$\ln(\tau_N(T)) = f_2(N, 1/k_B T). \tag{5}$$

These functions were constructed by fitting to the data points shown in Figs. 4 and 5, using ANNs again. In the case of D_N at 773 K, Fig. 6 shows both reference data points and the regression obtained using the ANN.
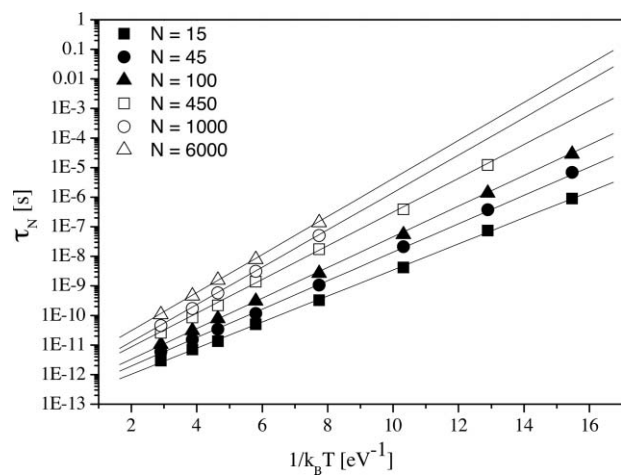

FIG. 5. Lifetimes τ_N of different vCu_N clusters versus reciprocal temperature ($1/k_B T$), measured with AKMC simulations. Plain lines show interpolation and extrapolation on the reciprocal temperature using f_2 defined in Eq. (5).
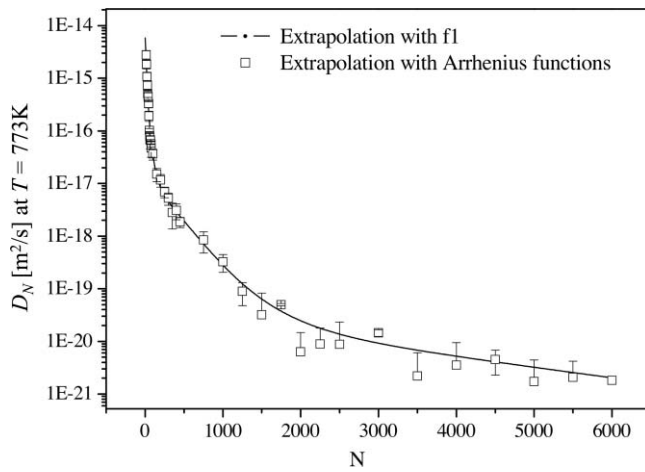
FIG. 6. Evolution of the diffusion coefficient D_N of vCu_N clusters with the number N of Cu atoms at 773 K. Dots show interpolation/extrapolation from AKMC data achieved with Arrhenius plots. The plain line shows interpolation/extrapolation achieved using function f_1 (Eq. (4)).

Finally, the probability p_N that the vCu_N cluster dissociates by the emission of a vCu_1 pair is simply calculated as the ratio between the number of times the clusters dissolved by this mechanism, and the number of times the vacancy alone was emitted. To obtain enough statistics, a number of simulations as large as 100 000 was necessary. These calculations could, therefore, only be performed at high temperature ($T \geq 1125$ K). The values we calculated are shown in Fig. 7. Similar to the above case, we designed a general fitting function based on ANN to extrapolate p_N to lower temperatures and to any size N:

$$p_N(T) = f_3(N, 1/k_B T) \tag{6}$$

Figure 7 shows the regression for 2000 K and its extrapolation to 773 K.

Overall, the CPU time required to produce the whole parameterization using an 8-core personal computer did not exceed two months, the training of the ANN being the least demanding part. This time can be significantly reduced, if more processors and/or faster computers are available.
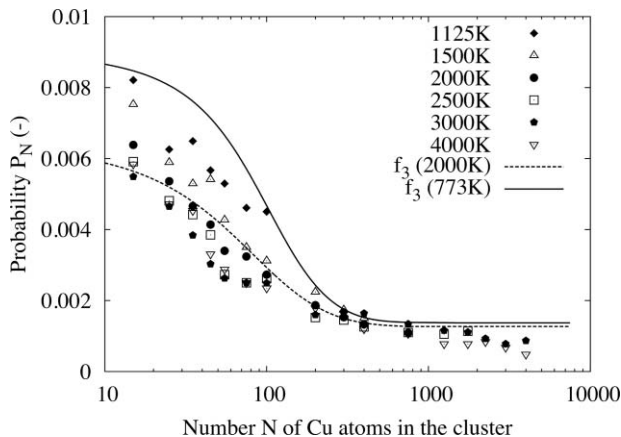

FIG. 7. Probability p_N for a vCu_N cluster to dissociate by the emission of a vCu_1 pair. Dots show the values calculated with 100 000 independent AKMC simulations at different temperatures. The dashed line shows interpolation using function f_3 (Eq. (6)) at 2000 K, and the plain line shows extrapolation using function f_3 at 773 K.

B. Time rescaling

Simulations of thermal annealing experiments with AKMC are conducted with the introduction of one vacancy in the simulation volume. The equilibrium vacancy concentration in real materials is, however, much smaller, by several orders of magnitude. For this reason, the Monte Carlo time t_{MC} must be rescaled before a comparison with experimental results is possible. This is a well-known problem that is formally solved by weighting the simulation time with the ratio between the vacancy concentration in the simulation box, $C_v^{(MC)}$, and the real vacancy concentration in the experiment, $C_v^{(real)}$,[7, 12–15]

$$t_{real} = t_{MC} \frac{C_v^{(MC)}}{C_v^{(real)}}. \tag{7}$$

The vacancy concentration in the simulation box is known exactly: it is the ratio between the number of vacancies (1 in our case) and the number of atoms N_{at}. However, Le Bouar and Soisson pointed out in Ref. 14 that this concentration should be corrected, in the case of solute atoms that, like Cu, interact strongly with the vacancy, with the fraction of time actually spent by the vacancy in Fe, i.e., far from Cu atoms. This is necessary because the binding of the vacancy with the Cu atoms will change locally the vacancy formation energy during the process of Cu precipitation. The effective vacancy concentration in the box is then precisely obtained as

$$C_v^{(MC)} = \frac{f_V}{N_{at} X_{Fe}}. \tag{8}$$

Here, X_{Fe} is the concentration of Fe atoms in the box ($X_{Fe} \approx 1$), and f_V is the fraction of time spent by the vacancy in a pure Fe environment, which can be exactly deduced from the simulation, by monitoring for how long the vacancy remains at a distance larger than second nearest neighbor separation from any Cu atom.[14]

Much more delicate is the estimation of the real vacancy concentration during the experiment (the experimental conditions used here for reference are listed in Table I). Given the enthalpy of formation of the vacancy in pure Fe, h_v^f (here we take $h_v^f = 1.7$ eV, because this is the value given by the interatomic potential used), after the correction of $C_v^{(MC)}$ with f_V, as described above, one can assume that the experimental vacancy concentration to be used as reference will be the equilibrium one in pure Fe, namely,

$$C_v^{(real)} \sim \exp\left(\frac{-h_v^f}{k_B T}\right) \tag{9a}$$

or

$$C_v^{(real)} = A \exp\left(\frac{-h_v^f}{k_B T}\right). \tag{9b}$$

Here, A is a coefficient that takes into account any deviation from the equilibrium concentration in pure Fe, due to the influence of Cu concentration (beyond second nearest neighbor distance) and also temperature (e.g., effect of vibrational entropy, not included in the model in any explicit or implicit way), as well as any other uncertainty inherent not only to the real experimental conditions (e.g., effect of impurities in the

TABLE I. Summary of the sets of experimental data used in this work, focusing on the coherent stage of precipitation (the average clusters radius $\bar{R} < 3$ nm). In the experimental technique column, APT stands for atom probe tomography, SANS for small angle neutron scattering, and SAXS for small angle x-rays scattering.

Cu content (at. %)	T (K)	Number of points	Max. cluster density (m^{-3})	Cluster density (m^{-3}) at $\bar{R} = 3$ nm	Expt. technique	Reference
1.34	773	3	1×10^{24}	$\sim 1 \times 10^{23}$	APT	Goodman *et al*. (Ref. 2)
1.34	773	6	4×10^{24}	$\sim 1 \times 10^{23}$	SANS	Kampmann and Wagner (Ref. 3)
1.34	773	3	2.5×10^{24}	$\sim 2 \times 10^{23}$	SANS	Mathon *et al*. (Ref. 5)
1.34	773	>10	…	…	SAXS	Perez *et al*. (Ref. 6)
1.34	873	>10	…	…		
1.34	973	>10	…	…		
1.1	823	4	$\sim 1.5 \times 10^{23}$	$\sim 1 \times 10^{23}$	SANS	Buswell *et al*. (Ref. 4)
0.6	773	6	2.7×10^{23}	$\sim 7 \times 10^{22}$	APT	Vincent *et al*. (Ref. 7)

alloy), but also to the choice, in the model, of a constant attempt frequency in Eq. (1). In the limit of infinite dilution and under fully ideal conditions, $A \approx 1$. Since A is not precisely known and cannot be calculated, we use it as fitting parameter for the comparison with experiments. This way of proceeding is equivalent to the one used by other authors, who rescaled time purely on empirical grounds, using the ratio between real and simulation time at the moment the simulation reached the experimental density of precipitates.[7] The advantage of our procedure is that the fitted value of A also acts as parameter of control, as it should not depart too much from a value of a few units, or of tens of units. The game rule is of course that a unique value of A must allow the reproduction of all data from the same experiment, i.e., for a given temperature and Cu content, both experimental precipitate density and mean size versus annealing time should be reproduced by the model for the same A value. As indicated in Table II, the values of A that allowed a comparison to be made between model predictions and experiments ranged from 0.77 to 10, which is fully acceptable.

III. SIMULATION OF THERMAL ANNEALING EXPERIMENTS

In this section, we report on the use of the hybrid AKMC approach described in Sec. II to simulate several thermal annealing experiments in Fe-Cu, as summarized in Table I. The results of our simulations are summarized in Table II and Fig. 8.

In order to choose the most appropriate simulation volume, as a trade-off between reasonable CPU time and statistical accuracy of the prediction, we consider that the peak of precipitate density is, at 773 K with 1.34 at. % Cu, of the order of 4×10^{24} m^{-3}. The density then decreases to 10^{23} m^{-3} at the end of coherent precipitation stage. A sufficient size for the AKMC simulation box is thus $64 \times 64 \times 64$ units cells (524 288 atoms), similar to other authors' choices.[7,15] The peak of density, if correctly predicted by the model, would then be reached by a number of 24 precipitates in the box, whereas if only one large precipitate remains at the end of the coherent stage the density will be still correctly sampled. Nonetheless, to obtain more statistics, some simulations were also conducted in a bigger box of $128 \times 128 \times 128$ unit cells (4 194 304 atoms). Another strategy adopted to optimize the CPU time has been to start the simulation with a smaller box and continue the same simulation in a box eight times bigger, when the densities become too low for the small box to provide enough statistics: this was achieved by duplicating the small box before restarting the simulation, an operation consistent with the use of periodic boundary conditions.

Figure 8 shows at a glance that the predictions of the hybrid AKMC model are in very good agreement with the experimental data (the corresponding values of A are given in Table II). For example, the increase of the average precipitate radius versus time in Fe-1.34 at. % Cu is very closely reproduced at all three temperatures investigated (773 K, 873 K, and 973 K). In the case of the experiment at 773 K, the measured evolution of the density of precipitates is also provided

TABLE II. Summary of the results obtained with the hybrid AKMC simulations performed in this work. N_{Cl} denotes the number of Cu clusters, and $\bar{R}$ the average cluster radius. The last simulation (Fe-1.1 at. % Cu at 823 K) was first started in a $64 \times 64 \times 64$ unit cells box, then interrupted and continued in a $128 \times 128 \times 128$ unit cells box when the number of clusters was lower than 10. The number of AKMC events is proportional to the CPU time.

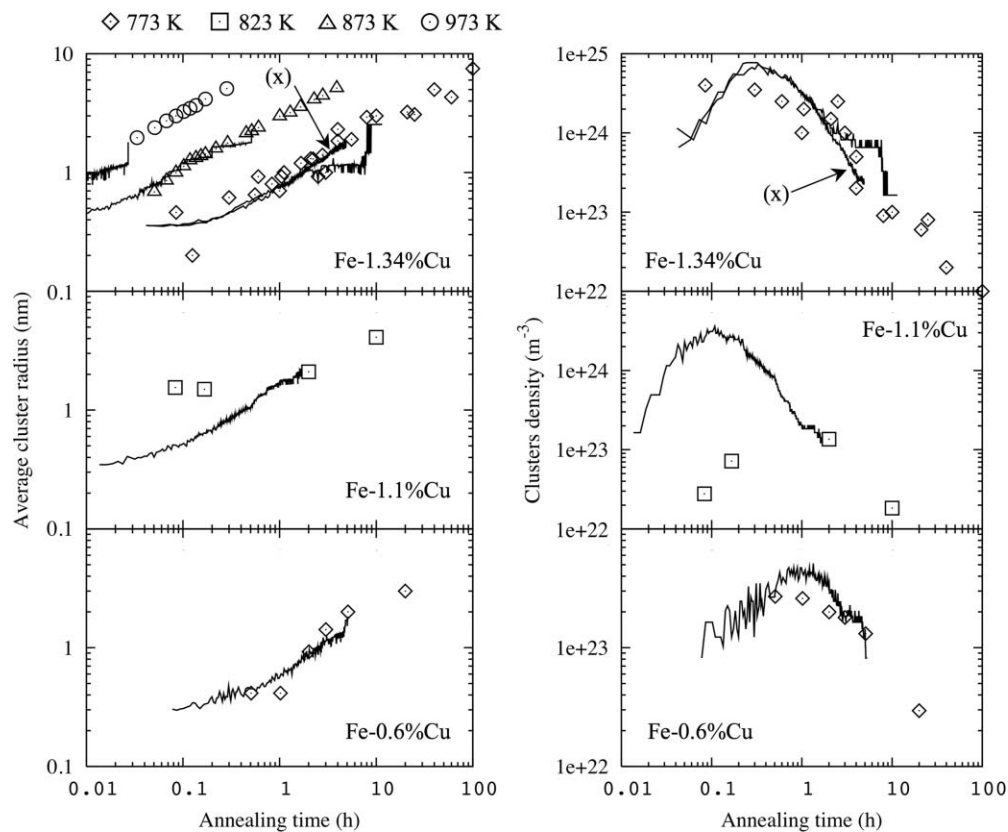| Cu content (at. %)	T (K)	AKMC box size (lattice units)	Number of AKMC events ($*1 \times 10^9$)	N_{Cl} at peak of density	N_{Cl}	$\bar{R}$ (nm)	f_V (Eq. (8))	A (Eq. (9b))
1.34	773	64	1.4	47	1	2.55	1.5×10^{-5}	1.7
1.34	773	128	4.2	375	11	1.76	1.5×10^{-5}	1.7
1.34	873	64	3.5	27	1	2.32	1.0×10^{-4}	1.7
1.34	973	64	6.3	9	1	1.9	8.1×10^{-4}	1.7
1.1	823	64/128	1.5/15.3	22 (in box 64)	6	2.17	4.4×10^{-5}	0.77
0.6	773	128	30.2	26	4	1.81	2.7×10^{-5}	10

FIG. 8. Comparison of the results of our hybrid AKMC simulations (plain lines) with experimental data (diamonds, squares, triangles, and circles) described in Table I. For the Fe-1.34 at. % Cu case at 773 K, the (x) mark indicates the results obtained in a $128 \times 128 \times 128$ unit cells box, whereas the unmarked one was obtained in a $64 \times 64 \times 64$ box.

and the model very nicely predicts nucleation (density increases), growth (density reaches a peak and remains temporarily constant, while the radius keeps increasing), and coarsening (density decreases, while the radius keeps increasing, because large precipitates grow at the expense of smaller ones). The curves obtained in the simulation box with sides of 64 lattice parameters are jerky because, especially when the coarsening stage is reached, only a few precipitates remain in the box and the disappearance of two small ones to make a bigger one produces significant oscillations in the overall density. In particular, step-like increases/decreases are observed: this is a clear indication of the fact that the mechanism leading to density decrease and radius increase is the coalescence of two mobile precipitates. Simulations conducted in the larger box (side of 128 lattice parameters) allow the jerks to be *damped*, thanks to better statistics (larger number of precipitates in the box). In all cases, the simulations finished with one single cluster in the box, of varying size, consistently with the increasing solubility limit with temperature.

The annealing of Fe-0.6 at. % Cu at 773 K leads to a precipitate density significantly smaller than the above case, at all stages, consistently with the halved solute concentration: the simulation could only be meaningfully performed in a $128 \times 128 \times 128$ unit cells box with $\sim 4 \times 10^{-6}$ atoms. These simulations were particularly demanding in terms of CPU time, most likely because the Cu concentration is lower and the acting thermodynamic force correspondingly weaker. Nonetheless, a good agreement with experimental data is achieved. The optimal A factor value, 10, is significantly

larger than for the more concentrated alloys. This may perhaps be the consequence of the assumption of constant attempt frequency Γ_0 in Eq. (1). For example, Soisson and Fu used two different attempt frequency values in Ref. 15, depending on the chemical nature of the jumping atom, larger for Fe than for Cu. Such a choice of different attempt frequencies may be a way to reduce this increase of A with decreasing concentration, because the proportion of Fe-vacancy exchanges is expected to increase if the Cu content is reduced.

In the simulation of the annealing of a Fe-1.1 at. % Cu alloy at 823 K we observe that the first two experimental points are not predicted by our model. The good agreement with
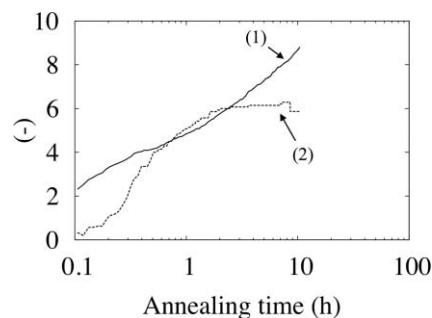

FIG. 9. Evolution with annealing time, during simulation with the hybrid AKMC, for a Fe-1.34 at. % Cu alloy at 773 K, of (1) the ratio between the total number of Cu atoms admitted in Cu clusters after their migration and the number of Cu atoms dragged by the vacancy from the matrix to the clusters vicinity and (2) the ratio between the number of vCu_N clusters objects merging and dissolutions.
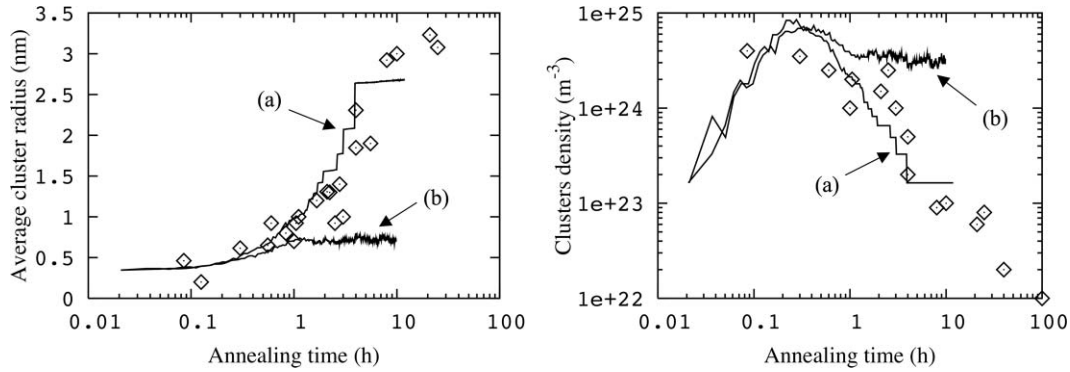
FIG. 10. Thermal annealing experiment for a Fe-1.34 at. % Cu alloy at 773 K. Parameters in the model were changed compared to Fig. 8: Curve (a) the probability p_N for vCu_N clusters objects to dissolve by the emission of a vCu_1 pair is set to 0. Curve (b) The vCu_N migration frequency $\Gamma_N^{(mig)}$ is modified to inhibit the migration of clusters bigger than 100 atoms.

experiments obtained in all other cases, however, gives us sufficient confidence to believe that those two experimental points are probably affected by large uncertainty, possibly as a consequence of the limited resolution of the experimental technique used, i.e., small angle neutron scattering, which is not sensitive to precipitates below 1 nm in diameter and therefore can be supposed to have overestimated the average size at the early stage of the precipitation, especially because in the experiment there was no support from any other complementary technique. This is confirmed by the fact that the third experimental point, still within the limit of coherent precipitation, is correctly reached by the model, and that a visual extrapolation of the curve will lead to reach the fourth point as well, even though this lies well into the regime where crystallographic transformation must have started, i.e., strictly speaking outside the range of validity of the model. Our model, as most experimental data, is roughly consistent with a dependence of the radius on a 1/2 power of time during growth, that decreases to a dependence on a 1/3 power of time during coarsening, as should be expected[6,7] (in logarithmic scale this is a roughly linear dependence, though with gradual change of slope), while no regression interpolating the four experimental points from Ref. 4 will respect such a law. Time was rescaled using an *A* factor value smaller than unity, perhaps a sign of experimental conditions significantly different from those of the other sets of experiments.

To summarize, the hybrid AKMC model proposed here is able to make relevant predictions of the kinetics of Cu precipitation in α-Fe, in an affordable CPU time on standard workstations. We thus believe that our model includes all important mechanisms of the investigated physical-chemical process and that these are satisfactorily parameterized. This achievement is of course also closely connected to the quality of the interatomic potential used, from which all parameters are obtained, either directly or indirectly.

IV. ANALYSIS OF THE Cu PRECIPITATION MECHANISM

Our results of Sec. III strongly support the idea that the mobility of Cu clusters and even precipitates plays a significant role in the process of precipitation in Fe, consistently

with the suggestion of Soisson and Fu[15] which, however, in their case could not be fully substantiated. With the algorithm we developed, it becomes possible to provide clear proof of this. Figure 9 shows the evolution with annealing time, in Fe-1.34 at. % Cu at 773 K, of: (1) the ratio between the number of Cu atoms absorbed in big clusters after their migration, and the number of Cu atoms dragged to the cluster absorption range by the vacancy and (2) the ratio between the number of times clusters density was reduced because of big clusters merging and because of clusters dissociation by the emission of CuV_1 pairs. These ratios are significantly larger than 1, and constantly increasing with time, confirming that indeed Cu clusters, in our simulations, grew mainly as a consequence of their migration and subsequent inclusion of Cu atoms, and that the clusters density decreased mainly due to the coalescence of mobile clusters. To further highlight this conclusion, we have conducted additional simulations (Fig. 10), in which some events were deliberately prohibited, namely, in one, the emission of vCu_1 pairs from vCu_N clusters was suppressed ($p_N = 0$); in the other, the migration frequency $\Gamma_N^{(mig)}$ was artificially modified in order to progressively inhibit the migration of the biggest vCu_N clusters (for $N > 100$). Compared to Fig. 8, when emission of vCu_1 is forbidden, the average precipitate radius is unsurprisingly somewhat larger and the average precipitate density almost unaltered, i.e., the results are virtually unaffected and remain in good agreement with experiments. When, however, Cu precipitate mobility is inhibited, the results deviate significantly from the experimental data: from a certain annealing time on, the average precipitate radius ceases to increase, and the clusters density ceases to decrease, thus remaining higher than the experimental one. Therefore, only by allowing large clusters to be mobile, the experimental results can be matched to the model. The one-by-one emission of vCu_1 pairs, on the contrary, is not a sufficiently efficient mechanism to enable coarsening as observed in experiments.

V. CONCLUSION

We have simulated the coherent stage of Cu precipitation in α-Fe during thermal annealing with novel hybrid atomistic kinetic Monte Carlo simulations. The vacancy migration

energies used to parameterize the model were calculated using a suitable interatomic potential, taking into account long-range chemical interactions and static relaxation, by exploiting the capabilities of artificial neural networks to interpolate and extrapolate the results of nudged elastic band calculations. This algorithm was hybridized with an object kinetic Monte Carlo approach, by treating Cu precipitates as objects above a certain size. The seamless matching between the atomistic and the coarse-grain approximations was ensured by calculating all parameters governing object behavior from atomistic simulations and again by exploiting the regression capability of artificial neural networks for extrapolation. This allowed the CPU time required by the simulations to be reduced by orders of magnitude and enabled complete thermal annealing experiments to be simulated, up to the end of the coherent precipitation stage, finding in addition very good agreement with the experimental data, both in terms of mean size and density of precipitates. This achievement proves: (1) the suitability of the interatomic potential used, which describes correctly not only the thermodynamic properties of the Fe-Cu system (phase diagram), but also the kinetics of precipitation and (2) that the model includes all important mechanisms driving the precipitation of Cu in iron. In particular, the coalescence of mobile Cu precipitates containing even several thousands of atoms (and one vacancy) turns out to be the dominant mechanism leading to growth and coarsening, while the classical coarsening mechanism based on the growth of larger clusters at the expense of dissolving small clusters (via emission of vCu_1 pairs) is clearly insufficient. This is consistent with what was proposed, though not fully proven, by Soisson and Fu.[15]

The hybrid model proposed here may seem somewhat specific for the problem of Cu precipitates; however, it appears to be suitable for interesting generalisation to all those cases in which coalescence of large, but mobile, nanofeatures is the main mechanism for their growth and coarsening. This is especially true for self-interstitial clusters that are formed under irradiation. The present model, therefore, paves the way for addressing more complex phenomena than thermal ageing, such as radiation-enhanced, or even induced, precipitation, not only in Fe-Cu, but also in more complex alloys.

ACKNOWLEDGMENTS

[1] G. R. Odette and G. E. Lucas, JOM **53**(7), 18 (2001).
[2] S. R. Goodman, S. S. Brenner, and J. R. Low, Metall. Trans. **4**, 2363 (1973).
[3] R. Kampmann and R. Wagner, in *Atomic Transport and Defects in Metals by Neutron Scatterings*, edited by C. Janot, W. Petry, D. Richter, and T. Springer (Springer, New York, 1986), p. 73.
[4] J. T. Buswell, C. A. English, M. G. Hetherington, W. J. Phythian, G. D. W. Smith, and G. M. Worrall, *Effects of Radiation on Materials: 14th International Symposium (Volume II)*, ASTM STP 1046, edited by N. H. Packan, R. E. Stoller, and A. S. Kumar (American Society for Testing and Materials, Philadelphia, 1990), pp. 127–153.
[5] M. H. Mathon, A. Barbu, F. Dunstetter, F. Maury, N. Lorenzelli, and C. H. de Novion, J. Nucl. Mater. **245**, 224 (1997).
[6] M. Perez, F. Perrard, V. Massardier, X. Kebler, A. Deschamps, H. de Monestrol, P. Pareige, and G. Covarel, Philos. Mag. **85**, 2197 (2005).
[7] E. Vincent, C. S. Becquart, C. Pareige, P. Pareige, and C. Domain, J. Nucl. Mater. **373**, 387 (2008).
[8] A. Deschamps, C. Genevois, M. Nicolas, F. Perrard, and F. Bley, Philos. Mag. **85**, 3091 (2005).
[9] S. I. Golubov, Y. N. Osetsky, A. Serra, and A. V. Barashev, J. Nucl. Mater. **226**, 252 (1995).
[10] S. I. Golubov, A. Serra, Y. N. Osetsky, and A. V. Barashev, J. Nucl. Mater. **277**, 113 (2000).
[11] F. Christien and A. Barbu, J. Nucl. Mater. **324**, 90 (2004).
[12] F. Soisson, A. Barbu, and G. Martin, Acta Mater. **44**, 3789 (1996).
[13] S. Schmauder and P. Binkele, Comput. Mater. Sci. **25**, 174 (2002).
[14] Y. Le Bouar and F. Soisson, Phys. Rev. B **65**, 094103 (2002), and references therein.
[15] F. Soisson and C. C. Fu, Phys. Rev. B **76**, 214102 (2007).
[16] F. Soisson, C. S. Becquart, N. Castin, C. Domain, L. Malerba, and E. Vincent, J. Nucl. Mater. **406**, 55 (2010), and references therein.
[17] C. S. Becquart and C. Domain, Phys. Status Solidi B **247**, 9 (2010).
[18] P. J. Othen, M. L. Jenkins, and G. D. W. Smith, Philos. Mag. A **70**, 1 (1994).
[19] S. Pizzini, K. J. Roberts, W. J. Phythian, C. A. English, and G. N. Greaves, Philos. Mag. Lett. **61**, 223 (1990).
[20] J. J. Blackstock and G. J. Ackland, Philos. Mag. A **81**, 2127 (2001).
[21] N. Castin and L. Malerba, J. Chem. Phys. **132**, 074507 (2010).
[22] H. Jónsson, G. Mills, and K. W. Jacobsen, in *Classical and Quantum Dynamics in Condensed Phase Simulations*, edited by B. J. Berne, G. Ciccotti, and D. F. Coker (World Scientific, Singapore, 1998).
[23] G. Henkelman and H. Jónsson, J. Chem. Phys. **113**, 9901 (2000).
[24] C. M. Bishop, *Neural Networks for Pattern Recognition* (Clarendon, Oxford, 1995).
[25] R. C. Pasianot and L. Malerba, J. Nucl. Mater. **360**, 118 (2007).
[26] N. Castin, L. Malerba, G. Bonny, M. I. Pascuet, and M. Hou, Nucl. Instrum. Methods Phys. Res. B **267**, 3002 (2009).
[27] C. Domain, C. S. Becquart, and L. Malerba, J. Nucl. Mater. **335**, 121 (2004).
[28] T. R. Mattsson, G. Mills, and H. Metiu, J. Chem. Phys. **110**, 12151 (1999).
[29] W. M. Young and E. W. Elcock, Proc. Phys. Soc. **89**, 735 (1966).
[30] B. Bortz, M. H. Kalos, and J. L. Lebowitz, J. Comput. Phys. **17**, 10 (1975).
[31] K. A. Fichthorn and W. H. Weinberg, J. Chem. Phys. **95**, 1090 (1991).
[32] M. I. Pascuet, N. Castin, and L. Malerba, J. Nucl. Mater. **412**, 106 (2011).